The Poly(dT)·2Poly(dA) Triple Helix

Frank B. Howard,* H. Todd Miles, and Philip D. Ross

Laboratory of Molecular Biology, National Institute of Diabetes and Digestive and Kidney Diseases, National Institutes of Health, Bethesda, Maryland 20892-0540

Received January 11, 1995; Revised Manuscript Received April 3, 1995[⊗]

ABSTRACT: A new homopolynucleotide triple helix, $(dT)_n{\cdot}2(dA)_n$, detected by circular dichroism mixing curves, is the product of an endothermic reaction of $(dA)_n{\cdot}(dT)_n$ with $(dA)_n$ at moderate temperatures and high salt concentrations ([NaCl] ≥ 2.6 M): $(dA)_n{\cdot}(dT)_n + (dA)_n \rightleftharpoons (dT)_n{\cdot}2(dA)_n$. At higher temperatures $(dT)_n{\cdot}2(dA)_n$ forms from the $(dA)_n{\cdot}(dT)_n$ duplex alone: $3[(dA)_n{\cdot}(dT)_n] \rightleftharpoons (dT)_n{\cdot}2(dA)_n + (dA)_n{\cdot}2(dT)_n$. Upon further heating, $(dT)_n{\cdot}2(dA)_n$ is converted to the triplex $(dA)_n{\cdot}2(dT)_n$: $2[(dT)_n{\cdot}2(dA)_n] \rightleftharpoons (dA)_n{\cdot}2(dT)_n + 3(dA)_n$. $(dT)_n{\cdot}2(dA)_n$ forms owing to a favorable entropy change; ΔH_m is unfavorable, ranging from 1 to 2.5 kcal mol^{-1}, depending upon [NaCl]. The formation reaction is associated with a negative change in heat capacity. $(dT)_n{\cdot}2(dA)_n$ is an extremely weak complex with a free energy of stabilization, $\Delta G° \leq 100$ cal mol^{-1}. T_m values of ultraviolet, circular dichroism, and differential scanning calorimetry transition curves for the formation of $(dT)_n{\cdot}2(dA)_n$ decrease with increasing [NaCl], reflecting, in part, the net uptake of cations. The values of $(dT_m/d \ln a_\pm)(\Delta H_m/RT_m^2)$ can be accounted for in terms of the charge spacing and cylindrical dimensions of the polynucleotides. The ionic strength dependence of this quantity is consistent with interaction of anions with (dA_n). High concentrations of the anions Cl^-, Br^-, and ClO_4^- decrease the stability of $(dT)_n{\cdot}2(dA)_n$ according to the lyotropic series. The highly polarizable anion, ClO_4^-, entirely prevents the formation of $(dT)_n{\cdot}2(dA)_n$. Phase diagrams of the $(dA)_n$,$(dT)_n$ system in solutions of NaCl, NaBr, and $NaClO_4$ are presented. A bonding scheme for $(dT)_n{\cdot}2(dA)_n$ is proposed, and implications of this work for Py·Pu·Pu triple helices are discussed.

Currently, there is renewed interest in the three-stranded polynucleotide helix owing to its possible role in cellular regulatory mechanisms and its potential therapeutic use by the control of transcription. Although polyribonucleotide triple helices have been known for more than thirty-five years (Felsenfeld *et al.*, 1957) and polydeoxyribonucleotide triple helices have been known for nearly thirty years (Riley *et al.*, 1966), some basic properties of these molecules have remained undetermined until recently. For example, $(dA)_n{\cdot}2(dT)_n$ was thought to exist as an A-form helix (Arnott & Selsing, 1974) but has been shown to assume the B-form (Howard *et al.*, 1992). In 1957 $(rA)_n{\cdot}2(rU)_n$ was first reported (Felsenfeld *et al.*, 1957), but formation of $(rU)_n{\cdot}2(rA)_n$ was not described until thirty years later, appearing to have gone undetected owing to a critical dependence on the size of $(rA)_n$ required for its formation (Broitman *et al.*, 1987).

In this paper, we report the formation of the new homopolynucleotide triple helix, $(dT)_n{\cdot}2(dA)_n$, by the endothermic conversion of $(dA)_n$ and $(dA)_n{\cdot}(dT)_n$ at high salt concentration ([NaCl] ≥2.6 M). Formation of $(dT)_n{\cdot}2(dA)_n$ is detected by means of circular dichroism (CD)[1] mixing curves, and the conditions of temperature and salt concentration at which $(dT)_n{\cdot}2(dA)_n$ is stable are determined by ultraviolet (UV) and CD thermal transition curves. We find that anions affect the stability of $(dT)_n{\cdot}2(dA)_n$ according to the lyotropic series. At a higher temperature near 60 °C, $(dT)_n{\cdot}2(dA)_n$ in [NaCl] ≥2.6 M is unstable and is converted to a mixture of the familiar triple helix, $(dA)_n{\cdot}2(dT)_n$, and $(dA)_n$. We also show that the double helix, $(dA)_n{\cdot}(dT)_n$, undergoes a novel thermally driven double disproportionation reaction at high [NaCl], resulting in formation of both of the possible triple helices: $(dT)_n{\cdot}2(dA)_n$ and $(dA)_n{\cdot}2(dT)_n$. The thermodynamic parameters associated with $(dT)_n{\cdot}2(dA)_n$ were obtained by differential scanning calorimetry (DSC) and used for analysis of the differential interaction of cations, anions, and water.

EXPERIMENTAL PROCEDURES

$(dA)_n$ (lot no. DE7836101, MW = 170 000; AG7836108, MW = 94 900; CJ7836106, MW = 29 500; and 3017836031, MW = 110 000) and $(dT)_n$ (lot no. CH78344103, MW 268 000; and 2067834032, MW = 61 000) were obtained from Pharmacia. Polymers were dissolved in deionized water. Solutions for UV and CD measurements were made by dilution of stock polymer solutions into buffer and salt solutions of appropriate concentration. Solutions for DSC measurements were prepared by weight dilution of polynucleotide master solutions and contained 0.01 M sodium cacodylate, pH 7.0, and NaCl of appropriate concentration. Polynucleotide concentrations were determined by absorption spectroscopy using molar extinction coefficients at UV maxima of $\epsilon = 8884 \pm 99$ L M^{-1} cm^{-1} for $(dA)_n$ and $\epsilon = 8460 \pm 79$ L M^{-1} cm^{-1} for $(dT)_n$ (0.002 M sodium cacodylate, pH 7.0, 0.1 M NaCl at 20 °C). These values were determined by replicate phosphorus analysis (Muraoka *et al.*, 1980).

UV melting curves were measured with a Cary Model 210 spectrophotometer interfaced to an IBM AT personal computer. Data were recorded with an acquisition program written by H. A. Fredrickson of the Division of Computer Research and Technology (DCRT), NIH. Data were transferred from the personal computer with program PC-NFS (Sun Microsystems) to a SUN SPARCstation 2 computer

[⊗] Abstract published in *Advance ACS Abstracts,* May 15, 1995.

[1] Abbreviations: CD, circular dichroism; DSC, differential scanning calorimetry; UV, ultraviolet.

for analysis with program LAP (Laboratory Analysis Package), written by J. I. Powell, J. Robinson, and J. T. Morris of DCRT, NIH.

CD spectra and CD melting curves were measured with a Jasco Model J-500A spectropolarimeter and recorded either with a personal computer using a commercial data acquisition program (Landis Instrument) modified by H. A. Fredrickson or with an LDACS computer system (Powell et al., 1980). Data were transferred to the SUN computer as described above. CD spectra are the average of five scans and have been smoothed and the base line corrected.

DSC measurements were carried out in a MicroCal MC-2 instrument equipped with 0.64 mL cells and operated at scan rates from 15 to 115 K h^{-1}. Polynucleotide solutions, 5−11 mM total [P], with their corresponding salt solutions as reference, were heated, usually at 60 K h^{-1}, to determine the excess heat capacity. A solvent *vs* solvent thermal scan was subtracted from the polynucleotide−solvent run to eliminate mismatch between the cells. All polynucleotide transitions were completely reversible; identical calorimetric traces were obtained upon reheating. DSC experiments were carried out in quadruplicate and were analyzed with the software program EXAM (Kirchoff, 1993). The pre- and post-transition asymptotic base lines are evaluated by a linear least squares fit using all of the data outside of the transition region. Maintaining these base-line parameters, the program then adjusts the number of moles, the molar enthalpy, and the midpoint temperature of the transition to obtain the best fit of a two-state model to the data in the transition region. The program also calculates a sigmoidal base line beneath the excess heat capacity peak, which is the transition progress curve normalized between the initial and final points of the transition. A stoichiometric coefficient appropriate for the molecularity of each reaction was used. In the analysis of highly asymmetric heat capacity envelopes, however, a value of this coefficient was chosen to give the best fit to the thermogram in order to obtain the best estimate of the progress base line. The calculation of the base line was the main goal of this computation. The calorimetric enthalpy of the reaction, ΔH_m, was obtained by integration of the measured heat capacity envelope over the calculated sigmoidal base line. The thermodynamic transition temperature, T_m, is the temperature at which the normalized extent of reaction is 0.5. There was no effect of concentration upon these thermodynamic parameters over the 2-fold range of concentration investigated.

RESULTS

Complexes Formed by $(dA)_n$ and $(dT)_n$. The combining ratio of interacting polynucleotides at a particular temperature and salt concentration may be determined by the method of continuous variation (Job, 1928). Polynucleotide complexes that form in the $(dA)_n$,$(dT)_n$ system in 3.4 M NaCl at 10, 46, and 72 °C are detected in the mixing curves (Job plots) of Figure 1, which are derived from CD spectra. At 10 °C, breaks in the mixing curve at 50 and 66.7 mol % $(dT)_n$ demonstrate formation of the double helix $(dA)_n$•$(dT)_n$ and the triple helix $(dA)_n$•2$(dT)_n$. At $(dT)_n \leq 50$ mol %, $(dA)_n$•$(dT)_n$ is the only complex that forms. Between 50 and 66.7 mol % $(dT)_n$, both $(dA)_n$•$(dT)_n$ and $(dA)_n$•2$(dT)_n$ can exist. Above 66.7 mol % $(dT)_n$, only $(dA)_n$•2$(dT)_n$ can form.

At 46 °C breaks in the mixing curve occur at 33.3 and 66.7 mol % $(dT)_n$, demonstrating formation of the new triple helix, $(dT)_n$•2$(dA)_n$, and of the more familiar triplex, $(dA)_n$•2$(dT)_n$. At $(dT)_n \leq 33.3$ mol %, $(dT)_n$•2$(dA)_n$ is the only complex possible. Between 33.3 and 66.7 mol % $(dT)_n$ both triple helices occur, the relative amounts depending upon the input ratio of $(dA)_n$ to $(dT)_n$. At $(dT)_n \geq 66.7$ mol %, $(dA)_n$•2$(dT)_n$ is the only complex that forms.

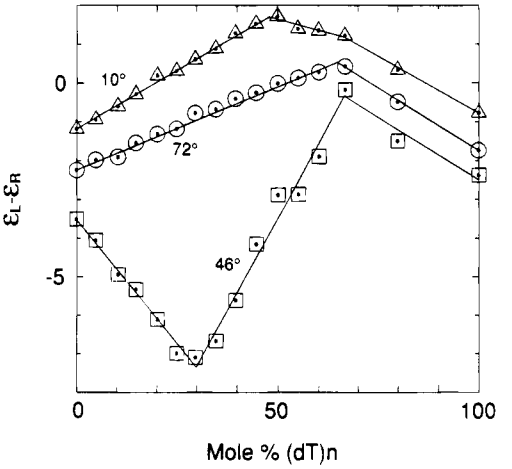

FIGURE 1: CD mixing curves for the $(dA)_n$,$(dT)_n$ system at 10 °C (△) (257 nm), 46 °C (⊡) (258 nm), and 72 °C (⊙) (254 nm). At 10 °C (△), $(dA)_n$•$(dT)_n$ and $(dA)_n$•2$(dT)_n$ are detected; at 46 °C (⊡), $(dT)_n$•2$(dA)_n$ and $(dA)_n$•2$(dT)_n$; and at 72 °C (⊙), only $(dA)_n$•2$(dT)_n$. The units of $\epsilon_L - \epsilon_R$ are L mol^{-1} cm^{-1}. Conditions: 3.4 M NaCl, 0.002 M sodium cacodylate, pH 7.0. These conditions apply to all succeeding figures unless noted otherwise.

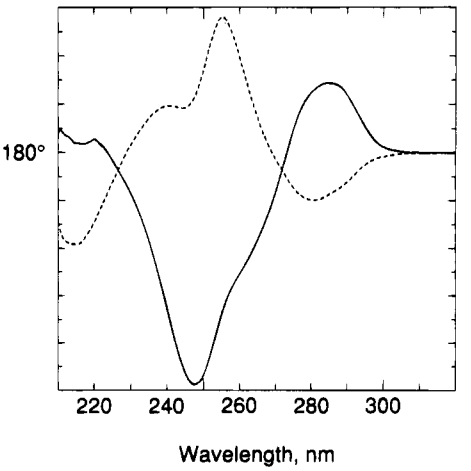

FIGURE 2: Wavelength dependence of the angles of intersection of CD mixing curves of the $(dA)_n$,$(dT)_n$ system at 46 °C. Optimum wavelengths for detecting $(dT)_n$•2$(dA)_n$ (solid line) are 247 and 285 nm; for $(dA)_n$•2$(dT)_n$ (dashed line), 255 and 280 nm. The departure from 180° (ordinate) is in arbitrary units of angle.

At 72 °C, three-stranded $(dA)_n$•2$(dT)_n$ is the only complex that can form. It is seen in Figure 1 that the new triple helix, $(dT)_n$•2$(dA)_n$, can form at the intermediate temperature of 46 °C but does not exist either at 10 °C or at 72 °C.

Optimum CD wavelengths for demonstrating specific complexes were determined from a computer-generated plot of wavelength against the angle of intersection of limbs of mixing curves for each complex (Howard *et al.*, 1976, 1984). For the $(dA)_n$,$(dT)_n$ system at 3.4 M NaCl and 46 °C, favorable wavelengths occur at 247, 254, and 282 nm (Figure 2). CD mixing curves plotted at these wavelengths, in Figure 3, unequivocally demonstrate formation of the new triple helix $(dT)_n$•2$(dA)_n$ as well as the other possible triplex $(dA)_n$•2$(dT)_n$.

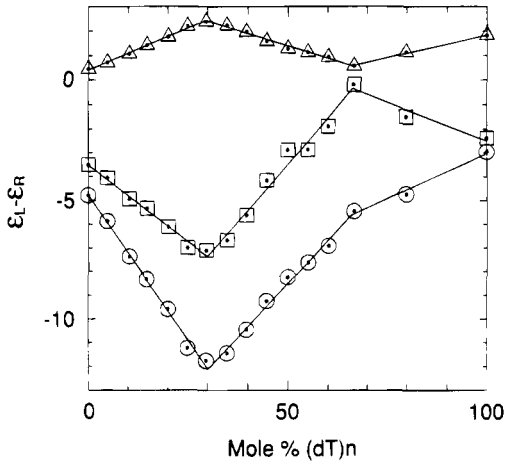

FIGURE 3: CD mixing curves (46 °C) at the favorable wavelengths 247 nm (⊙), 254 nm (⊡), and 282 nm (△). All detect formation of the new triple helix (dT)$_n$•2(dA)$_n$ as well as (dA)$_n$•2(dT)$_n$. $\epsilon_L - \epsilon_R$ values at 247 nm and at 254 nm have been decreased by 1.5 and by 1, respectively, for clarity of presentation.

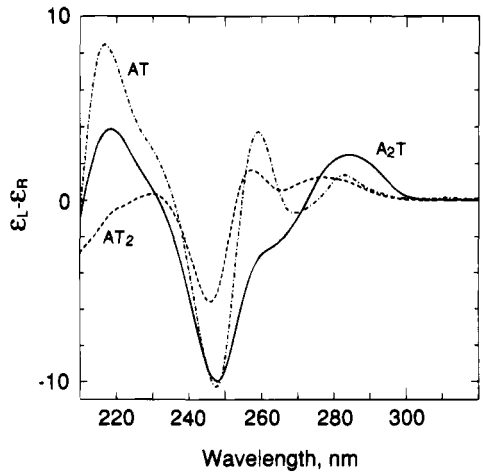

FIGURE 4: CD spectra of (dT)$_n$•2(dA)$_n$ at 28 °C (solid line), (dA)$_n$•(dT)$_n$ at 10 °C (dot-dashed line), and (dA)$_n$•2(dT)$_n$ at 28 °C (dashed line). (dA)$_n$•2(dT)$_n$ was measured in 4.0 M NaCl, 0.002 M sodium cacodylate, pH 7.0.

CD Spectra of Complexes in the (dA)$_n$,(dT)$_n$ System at High NaCl Concentration. CD spectra of the three complexes (dA)$_n$•(dT)$_n$, (dT)$_n$•2(dA)$_n$, and (dA)$_n$•2(dT)$_n$ are shown in Figure 4; they were taken under conditions at which only one complex was present. Each complex has a distinct and characteristic CD spectrum, a property that we employ for establishing which complexes are present under various experimental conditions. The spectrum of the new complex, (dT)$_n$•2(dA)$_n$, has maxima at 218 and 282 nm, a shoulder near 260 nm, and a deep minimum at 248 nm. Characteristic shapes of these spectra vary little with temperature; however, marked spectral changes appear when transitions occur and the composition of the complexes changes.

Thermally Induced Transitions. Upon heating, the various polynucleotide complexes of (dA)$_n$ and (dT)$_n$ undergo cooperative transformation reactions. CD melting curves are shown in Figure 5 for solutions at 1:2, 2:1, and 1:1 mole ratios of (dA)$_n$ to (dT)$_n$.

In the 2A:1T mixture in 3.4 M NaCl, two transitions occur, one beginning near 10 °C and the other near 60 °C (middle curve, Figure 5). The mixing curves of Figures 1 and 3 have demonstrated that the (dT)$_n$•2(dA)$_n$ complex is present at 46

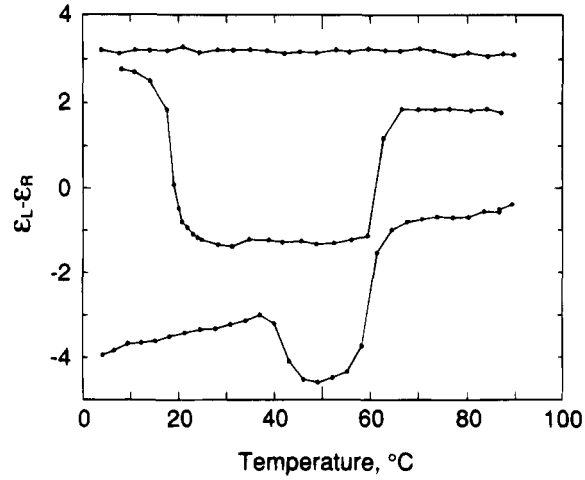

FIGURE 5: CD thermal transitions at different mole ratios: (dA)$_n$,(dT)$_n$ (1:2) (257 nm, top), (dT)$_n$,(dA)$_n$ (1:2) 257 nm, middle), and (dA)$_n$,(dT)$_n$ (1:1) (247 nm, bottom). All solutions contained 0.12 mM polymer P; the top curve was measured at 4.0 M NaCl, 0.002 M sodium cacodylate, pH 7.0. Ordinate values have been increased by 1.5, 1, and 3 for the top, middle, and bottom curves, respectively. T_m's are 18.7 °C and 61.8 °C for the middle curve and 42.5 °C and 59.9 °C for the bottom curve.

°C but not at 10 °C or at 72 °C. That the CD spectrum of this mixture changes only slightly between 25 and 60 °C and has the characteristic shape of (dT)$_n$•2(dA)$_n$, shown in Figure 4, indicates that (dT)$_n$•2(dA)$_n$ is the complex present in the temperature region between the two transitions. The mixing curve measured at 10 °C (Figure 1) establishes the composition of the 2A:1T mixture at the lower plateau of the first transition as (dA)$_n$•(dT)$_n$ + (dA)$_n$. Since the composition at the upper plateau is (dT)$_n$•2(dA)$_n$, the low temperature transition may be identified as

$$(dA)_n\text{•}(dT)_n + (dA)_n \rightleftharpoons (dT)_n\text{•}2(dA)_n \quad (1)$$

The (dT)$_n$•2(dA)$_n$ triple helix undergoes a second transition near 60 °C (Figure 5, middle curve). The mixing curve measured at 72 °C (Figure 1) indicates that (dA)$_n$•2(dT)$_n$ is the only complex present at this temperature. The high temperature (T_m = 60 °C) transition, therefore, represents the conversion of one kind of triple helix to another. This obviously complex process may be summarized by the overall reaction scheme

$$2[(dT)_n\text{•}2(dA)_n] \rightleftharpoons (dA)_n\text{•}2(dT)_n + 3(dA)_n \quad (2)$$

At a 1:1 (dA)$_n$ to (dT)$_n$ ratio at 10 °C, the mixing curve of Figure 1 shows that the double helix is the sole form present. With increasing temperature, the CD spectrum of (dA)$_n$•(dT)$_n$ (Figure 4) changes, and at the end of the first transition at 42.5 °C (Figure 5, bottom curve), the spectrum of a 1:1 mixture is the same as a summation of the separately measured spectra of the two triple helices (Figure 6). This result is consonant with the mixing curves measured at 46 °C (Figures 1 and 3), which show that both triple helices can exist. The 42 °C transition is a new and unusual disproportionation of a double helix to form two triple helices that is represented by the overall equation

$$3[(dA)_n\text{•}(dT)_n] \rightleftharpoons (dT)_n\text{•}2(dA)_n + (dA)_n\text{•}2(dT)_n \quad (3)$$

As further confirmation of this assignment, we have meas-

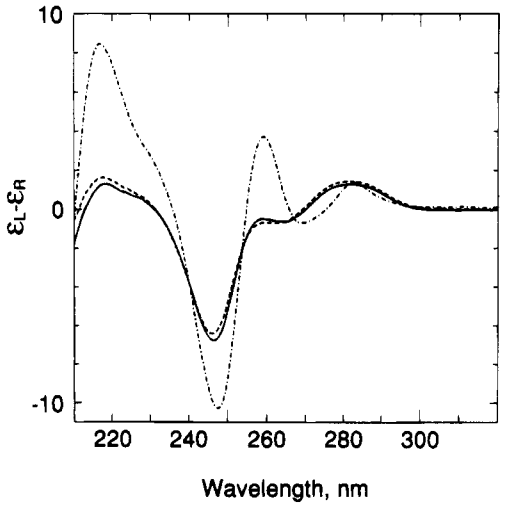

FIGURE 6: CD spectra of $(dA)_n$,$(dT)_n$ (1:1) at 10 °C (dot-dashed line) and at 46 °C (solid line), and of a weighted summation (1:1) of $(dT)_n$•2$(dA)_n$ and $(dA)_n$•2$(dT)_n$ at 46 °C (dashed line).

ured the CD spectrum of a 1:1 $(dA)_n$ to $(dT)_n$ mixture prepared by an alternate route, namely, by adding $(dT)_n$ to preformed $(dT)_n$•2$(dA)_n$. This CD spectrum is identical to the summation spectrum of the two triple helices (Figure 6) but differs markedly from a summation of the separately measured spectra of $(dA)_n$ and $(dT)_n$•2$(dA)_n$ (data not shown). The equilibrium state of a 1:1 $(dA)_n$ to $(dT)_n$ mixture, under these conditions, whether made by adding $(dA)_n$ directly to $(dT)_n$ or by adding $(dT)_n$ to $(dT)_n$•2$(dA)_n$, thus consists of a 1:1 mixture of the two triple helices. Upon further heating of this 1:1 mixture of triple helices, the less stable $(dT)_n$•2$(dA)_n$ is converted to the familiar $(dA)_n$•2$(dT)_n$ triple helix by the same reaction scheme (eq 2) and at the same temperature of 60 °C as in the 2A:1T case (bottom curve, Figure 5).

At a 1:2 $(dA)_n$ to $(dT)_n$ ratio, the $(dA)_n$•2$(dT)_n$ triple helix is formed at low temperature (Figure 1); its spectrum (Figure 4) remains virtually unchanged upon heating, resulting in the flat thermal profile of the 257 nm CD signal (top curve of Figure 5) which shows that $(dA)_n$•2$(dT)_n$ is stable to above 90 °C under these conditions (4.0 M NaCl).

Differential Scanning Calorimetry. The DSC behavior of $(dT)_n$•2$(dA)_n$ is shown in Figure 7. The low temperature endothermic peak represents the formation of the $(dT)_n$•2$(dA)_n$ complex from $(dA)_n$ and $(dA)_n$•$(dT)_n$ according to eq 1. The transition temperature at which this reaction takes place decreases from approximately 37 to 20 °C as the salt concentration is raised from 2.6 to 3.1 M NaCl and the shape of the transition becomes increasingly asymmetric and steeper on the low temperature side. The best fit to the DSC trace is to a two-state dimer association model at 37 °C in 2.6 M NaCl, corresponding to the reaction as written in eq 1. A tetramer association model best fits the shape of the DSC trace obtained in 3.4 M NaCl at 16 °C. Examination of the low temperature transition for any kinetic influence proved negative: experiments carried out at scanning rates from 15 to 115 K h^{-1} yielded identical ΔH_m's (integrated areas) and T_m's for the formation of $(dT)_n$•2$(dA)_n$ taking place between 37 and 12 °C in 2.6−3.7 M NaCl.

The thermodynamics the formation of $(dT)_n$•2$(dA)_n$ by eq 1 are characterized t a small positive enthalpy change and a marked negative h t capacity change (Table 1). The endothermic ΔH_m values for the formation of $(dT)_n$•2$(dA)_n$

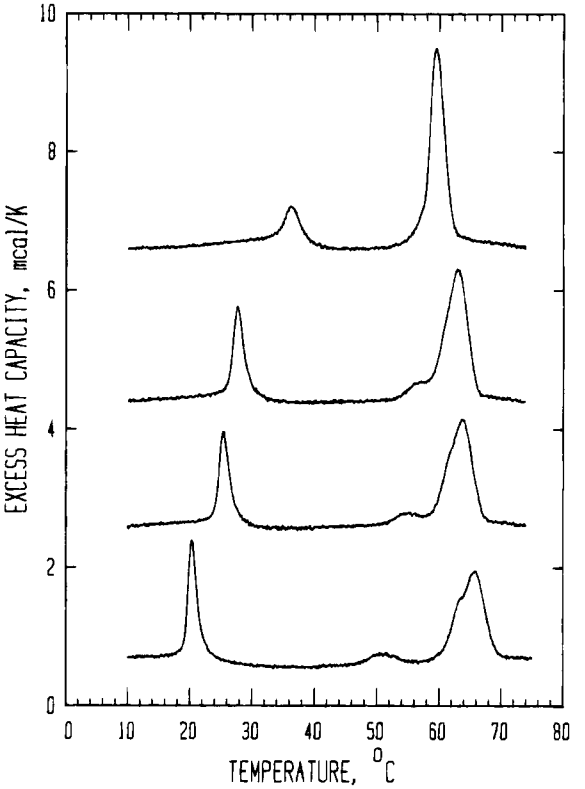

FIGURE 7: DSC curves at mole fraction $(dA)_n$ = 0.634 (top to bottom) in 2.6, 2.8, 2.9, and 3.1 M NaCl, respectively. Solutions contain 0.01 M sodium cacodylate, pH 7.0. Ordinate arbitrarily displaced for presentation.

are between 1 and 2.5 kcal mol^{-1}; the associated changes in entropy which drive this reaction range between 3.5 and 9 cal K^{-1} mol^{-1} as the salt concentration is increased from 2.6 to above 3.3 M NaCl. Analysis of the pre- and post-transition base lines of the individual DSC traces (Figure 7) shows that the formation of $(dT)_n$•2$(dA)_n$ is accompanied by a decrease in heat capacity: $\Delta C_p = -90 \pm 11$ cal K^{-1} mol^{-1} (Table 1), not differing significantly from the value of $\Delta C_p = -68 \pm 18$ cal K^{-1} mol^{-1} obtained from the slope of the regression of ΔH_m as a function of temperature. ΔC_p appears to diminish at high salt and low temperature.

The transitions shown in Figure 7 taking place at higher temperatures, after the formation of $(dT)_n$•2$(dA)_n$, are all complex processes involving more than one reaction step. At mole percent $(dA)_n$ = 63.4, as a consequence of the departure from the 2A:1T ratio, a small amount of $(dA)_n$•$(dT)_n$ is present as well as $(dT)_n$•2$(dA)_n$. A separate transition breaks off from the main high temperature peak as the salt concentration increases and may be seen in Figure 7 to be discrete and centered just above 50 °C in 3.1 M NaCl. This transition arises from the novel double disproportionation of $(dA)_n$•$(dT)_n$ (eq 3), resulting in the formation of two triple helices. A value of ΔH_m = 4 kcal mol^{-1} is associated with this process and is independent of NaCl concentration and temperature (Table 1).

The major high temperature transition is the triple helix conversion reaction in which $(dT)_n$•2$(dA)_n$ → $(dA)_n$•2$(dT)_n$, as written in eq 2. This transition develops a shoulder in 2.9 M NaCl, which becomes more articulated in 3.1 M NaCl (Figure 7). DSC traces obtained at $(dA)_n$ = 68.5 mol % (data not shown) do not show the intermediate transition due to eq 3 because no $(dA)_n$•$(dT)_n$ is present; however, the

Table 1: Thermodynamic Parameters of (dT)$_n$•2(dA)$_n$ in NaCl from Calorimetry

		reaction[a]							
		A + AT = A_2T				3AT = A_2T + AT_2		2A_2T = AT_2 + 3A	
Na^+ (M)	x_A[b]	T_m (°C)	ΔH_m (kcal/mol)[c]	ΔS_m (eu)[d]	ΔC_p (eu)[e]	T_m (°C)	ΔH_m (kcal/mol)	T_m (°C)	ΔH_m (kcal/mol)
2.60	0.634	36.90	1.07	3.45	−91			59.5	7.36
2.68	0.685	32.59	1.15	3.76	−108			61.2	6.32
2.81	0.634	28.11	1.87	6.21	−90	56.5	4.07	63.0	7.81
2.89	0.685	26.01	1.75	5.85	−98			63.2	6.84
2.91	0.634	25.87	2.03	6.78	−97	54.6	3.95	63.9	7.37
3.09	0.685	21.44	2.17	7.37	−115			64.7	8.24
3.12	0.634	20.65	2.42	8.24	−84	50.1	3.93	63.4	7.63
								65.5	
3.38	0.509					42.5	3.87	63.6	7.20
3.40	0.634	16.27	2.67	9.23	−87	46.3	4.25	64.6	7.60
								67.1	
3.41	0.685	16.26	2.37	8.19	−72			66.1	7.58
3.72	0.685	12.19	2.60	9.11	−63			67.3	6.90
3.74	0.509					36.2	4.34	65.7	6.72
mean ± 95% confidence interval[f]					−90 ± 11		4.07 ± 0.20		7.30 ± 0.34

[a] Values in the table refer to 1 mol of reaction as written. [b] x_A is mole fraction (dA)$_n$. [c] For the first two entries, two standard errors of the mean was ±20 cal mol^{-1} and for the rest was ±60 cal mol^{-1}. [d] eu = cal mol^{-1} K^{-1}. [e] The average two standard errors of the mean for each entry was ±8 eu. [f] Confidence interval was constructed with the t statistic.

higher temperature transition exhibits the same tendency toward bimodal appearance shown in the two traces at the bottom of Figure 7. In 3.7 M NaCl at a scan rate of 16.5 K h^{-1}, ΔH_m was identical to the value determined at 60 Kh^{-1}; however, both peaks of the higher temperature transition were 1 °C lower, indicating kinetic effects in this transition. Owing to the complex nature of the reaction, no attempts were made at kinetic analysis or decomposition of the bimodal thermograms.

Dependence of Thermal Transitions upon Na^+ and Anion Concentration. UV melting profiles of 2:1 (dA)$_n$ to (dT)$_n$ mixtures as a function of NaCl concentration are given in Figure 8. Phase diagrams of the (dA)$_n$,(dT)$_n$ system in NaCl, NaBr, and $NaClO_4$ are shown in Figure 9. These diagrams are derived primarily from UV melting curves, although CD data are used at high NaCl and NaBr concentrations where (dT)$_n$•2(dA)$_n$ is involved. The behavior of the system at high concentrations of NaCl is shown in greater detail in Figure 10 so that the T_m's determined by the CD, UV, and DSC techniques may be compared. It is seen (Figures 7−10) that T_m for the formation of (dT)$_n$•2(dA)$_n$ decreases as the salt concentration increases. The temperature interval in which (dT)$_n$•2(dA)$_n$ is stable broadens with higher [NaCl] (Figures 8−10). (dT)$_n$•2(dA)$_n$ does not form below 2.6 M NaCl (bottom curve of Figure 8; Figures 9 and 10), nor does it form at all in $NaClO_4$ (Figure 9). An inverse dependence of transition temperature upon salt concentration is also observed (Figure 9 and 10) for the formation of (dT)$_n$•2(dA)$_n$ and (dA)$_n$•2(dT)$_n$ from the (dA)$_n$•(dT)$_n$ double helix (eq 3). T_m for the transition converting (dT)$_n$•2(dA)$_n$ to (dA)$_n$ and (dA)•2(dT)$_n$ (eq 2) increases nonlinearly with increasing [NaCl] (Figure 10). T_m for the dissociation of (dA)$_n$•2(dT)$_n$ is >90 °C for NaCl >1.2 M, and no transition ascribable to melting of this triple helix is likely for [NaCl] ≥2.6 M. The CD thermal profile monitoring $\Delta\epsilon$ at 257 nm (top curve, Figure 5) confirms that the dissociation of (dA)$_n$•2(dT)$_n$ is not observed at high NaCl concentration.

Differential Interaction Parameters. Combining the observed dependence of T_m upon salt concentration and ΔH_m, the measured calorimetric enthalpy changes, we have calculated values of a parameter, Z, that is related by theory

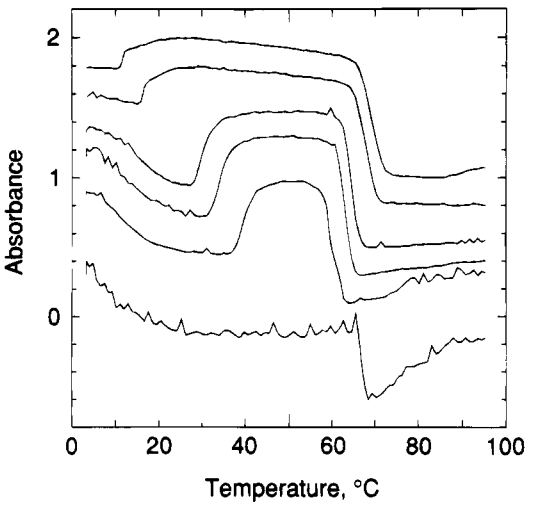

FIGURE 8: UV thermal profiles of (dT)$_n$,(dA)$_n$ (1:2 ratio) at 280 nm in 4.0, 3.6, 3.0, 2.8, 2.6, and 2.2 M NaCl (top to bottom). T_m's are 11.9 °C and 69.1 °C; 16.8 °C and 67.7 °C; 30.4 °C and 64.4 °C; 34.4 °C and 63.0 °C; 40.0 °C and 59.7 °C; 66.7 °C (top to bottom). No low temperature transition is observed in the bottom curve because (dT)$_n$•2(dA)$_n$ does not form in 2.2 M NaCl. Polymer concentration was 0.18 mM P for all samples. To recover the original absorbance values, the three factors in parentheses (one set per curve) should be subtracted, multiplied, and added in turn to each curve shown above: (1, 0.1332, 0.4958), (0.8, 0.1351, 0.4789), (0.4, 0.1239, 0.4692), (0.3, 0.1263, 0.4791), (0.1, 0.1231, 0.4782), (−0.6, 0.0772, 0.4720) (top to bottom, respectively).

(Record *et al.*, 1978) to the differential number of moles of cations, of anions, and of water that are associated with each helix transformation process. The exact significance of Z is deferred to eq 7 below. We calculate Z as an empirical quantity as the product of our observables

$$Z = \left(\frac{dT_m}{d \ln a_\pm}\right)\left(\frac{\Delta H_m}{RT_m^2}\right) \quad (4)$$

The activity, $a_\pm$, of the salt was calculated from the molality of the salt solution and the mean molal activity coefficients, determined at each salt concentration and T_m from the fitting equations of Archer (1992) in a convenient computer

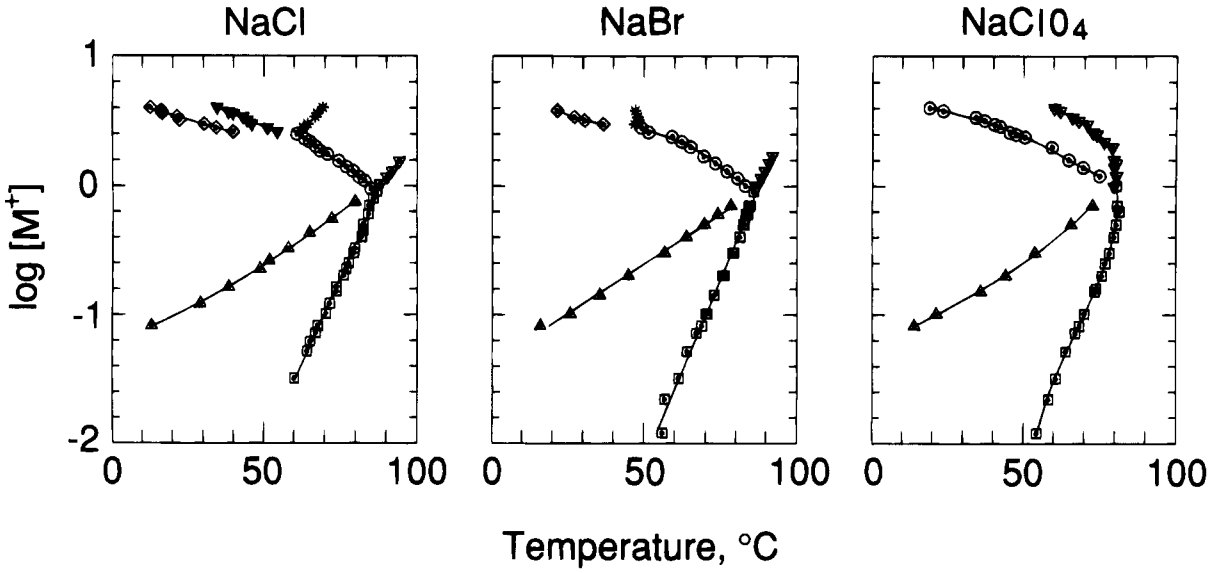

FIGURE 9: Phase diagrams for the $(dA)_n$,$(dT)_n$ system in solutions of NaCl (left), NaBr (center), and $NaClO_4$ (right). Data are from UV and CD melting curves. Previously described transitions are as follows: $(dA)_n$•$(dT)_n$ ⇌ $(dA)_n$ + $(dT)_n$ (⊡); $(dA)_n$•$2(dT)_n$ ⇌ $(dA)_n$•$(dT)_n$ + $(dT)_n$ (△); $(dA)_n$•$2(dT)_n$ ⇌ $(dA)_n$ + 2 $(dT)_n$ (dotted ▽); $2[(dA)_n$•$(dT)_n]$ ⇌ $(dA)_n$•$2(dT)_n$ + $(dA)_n$ (⊙)). New transitions are as follows: $(dA)_n$•$(dT)_n$ + $(dA)_n$ ⇌ $(dT)_n$•$2(dA)_n$ (dotted ◇); $3[(dA)_n$•$(dT)_n]$ ⇌ $(dA)_n$•$2(dT)_n$ + $(dT)_n$•$2(dA)_n$ (▼); $2[(dT)_n$•$2(dA)_n]$ ⇌ $(dA)_n$•$2(dT)_n$ + $3(dA)_n$ (*). A:T ratios are as follows: 1:1 (⊡, ⊙, ▼); 1:2 (△, dotted ▽); and 2:1 (dotted ◇, *).

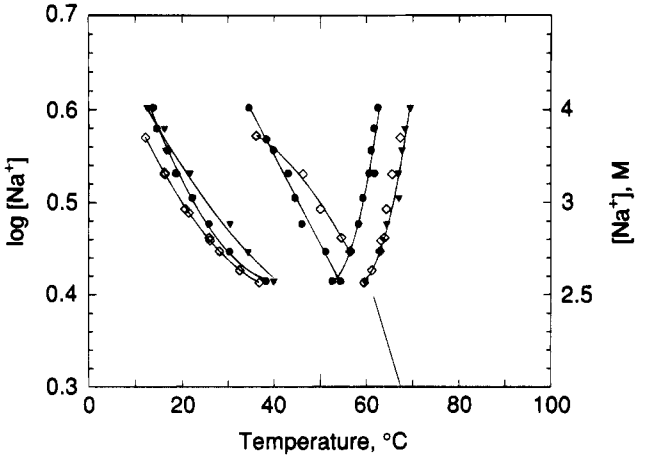

FIGURE 10: Comparison of phase diagrams (2.6−4.0 M NaCl) obtained by UV (▼); CD (●), and DSC (◇) methods. Shown in greater detail are the new transitions: $(dA)_n$ + $(dA)_n$•$(dT)_n$ ⇌ $(dT)_n$•$2(dA)_n$ (left three curves); $3[(dA)_n$•$(dT)_n]$ ⇌ $(dT)_n$•$2(dA)_n$ + $(dA)_n$•$2(dT)_n$ (center two curves); $2[(dT)_n$•$2(dA)_n]$ ⇌ $(dA)_n$•$2(dT)_n$ + $3(dA)_n$ (right two curves). Part of the 2 → 3 transition, $2[(dA)_n$•$(dT)_n]$ ⇌ $(dA)_n$•$2(dT)_n$ + $(dA)_n$, is shown at the bottom (solid line). Only about half of the UV and CD data are shown. Equations fitted to the entire data sets are as follows: log [Na^+] = $0.813 - 0.0190T_m + 0.00225T_m^2$ (●, left); log [Na^+] = $0.727 - 0.0111T_m + 0.00008T_m^2$ (▼, left); log [Na^+] = $0.716 - 0.0139T_m + 0.00015T_m^2$ (◇, left); log [Na^+] = $0.938 - 0.00965T_m$ (●, center); log [Na^+] = $0.490 + 0.00778T_m - 0.000152T_m^2$ (◇, center); log [Na^+] = $4.543 - 0.1596T_m + 0.001543T_m^2$ (●, right); log [Na^+] = $5.760 - 0.1833T_m + 0.001572T_m^2$ (▼, right).

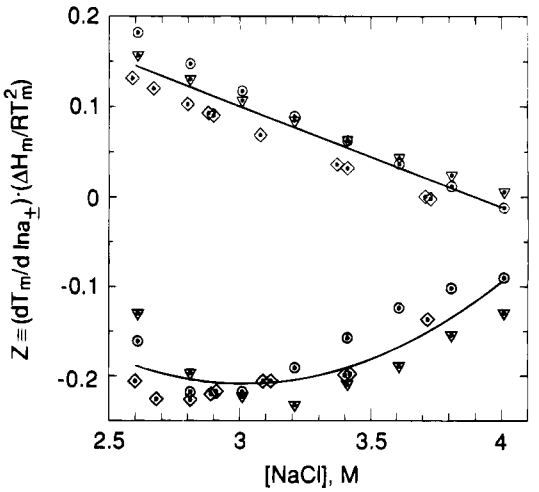

FIGURE 11: Dependence of $(dT_m/d \ln a_\pm)(\Delta H_m/RT_m^2)$ on [NaCl] for the reactions $2[(dT)$•$2(dA)_n]$ ⇌ $(dA)_n$•$2(dT)_n$ + $3(dA)_n$ (top) and $(dA)_n$ + $(dA)_n$•$(dT)_n$ ⇌ $(dT)_n$•$2(dA)_n$ (bottom). Data were obtained from UV (dotted ▽), CD (⊙), and DSC (dotted ◇) measurements of T_m, and DSC measurements of ΔH_m.

program format. The mean molal activity coefficients, $\gamma_\pm$, were in the range of 0.70−0.77 for 2.6−3.7 M NaCl at various temperatures between 12 and 66 °C. Values of $(dT_m/d \ln a_\pm)$ were obtained from the lowest order polynomial in $\ln a_\pm$ best fitting the T_m values from the CD, UV, and DSC techniques. In the calculation of Z for the process in eq 1, ΔH_m (per nucleotide phosphate) was expressed as a cubic function of molality. The values of Z for the formation of $(dT)_n$•$2(dA)_n$ according to eq 1 and its high temperature transformation according to eq 2 are shown in Figure 11 to depend upon NaCl concentration. In contrast, the values of Z for the double disproportionation reaction of $(dA)_n$•$(dT)_n$ (eq 3) are nearly independent of [NaCl] and are −0.10 from CD and −0.16 from DSC measurements, this difference arising from the different observed dependence of T_m upon [NaCl] (Figure 10).

DISCUSSION

We have reported the discovery of the new homopolynucleotide triple helix, $(dT)_n$•$2(dA)_n$, the conditions under which it forms, and the novel transformation reactions in which it participates. These findings were made possible by the distinct CD spectral characteristics of the different complexes formed in the $(dA)_n$,$(dT)_n$ system. We have used mixing curves, melting curves, and the summation of catalog spectra to identify the composition of mixtures under different environmental conditions. Phase diagrams sum-

marizing the thermal stability of complexes in the (dA)$_n$,(dT)$_n$ system in NaCl, NaBr, and $NaClO_4$ solutions, derived from UV melting curves and CD melting curves (when (dT)$_n$•2(dA)$_n$ is present), are shown in Figure 9.

Comparison of Transition Temperatures from CD, DSC, and UV Measurements. T_m's associated with (dT)$_n$•2(dA)$_n$ at identical high NaCl concentrations as observed by DSC, UV, and CD spectroscopy differ significantly (Figure 10) from one another. The three methods, however, monitor different aspects of the same transition. In the formation of (dT)$_n$•2(dA)$_n$ at low temperature, the CD transition takes place after the calorimetric transition is complete. At high temperature, the CD transition of (dT)$_n$•2(dA)$_n$ to (dA)$_n$•2(dT)$_n$ is about 7 °C lower and is essentially complete by the beginning of the DSC transition. The CD transition, thus, appears to monitor the perturbation of the perfected (dT)$_n$•2(dA)$_n$ helical structure by reflecting the initial deviations from the highly characteristic (Figure 4) CD spectrum of that complex. DSC provides a true thermodynamic transition temperature (in contrast to the midpoint of the change in a spectral signal), and the shape of the DSC plot is an extremely sensitive indicator of the complex nature of these transformations. This complexity is reflected in the bimodal and asymmetric appearance of the excess heat capacity traces. The transitions monitored by UV spectral changes primarily reflect the incorporation of single-stranded (dA)$_n$ into the various helical complexes. Consistent with this interpretation, the novel double disproportionation reaction of (dA)$_n$•(dT)$_n$ to the two triple helices, (dA)$_n$•2(dT)$_n$ and (dT)$_n$•2(dA)$_n$ (eq 3), was not detectable by UV.

The differences between these three techniques are much more pronounced at high salt concentration than we find for the simpler transitions of the (dA)$_n$,(dT)$_n$ system (e.g., (dA)$_n$•2(dT)$_n$ → (dA)$_n$ + 2(dT)$_n$, (dA)$_n$•(dT)$_n$ → (dA)$_n$ + (dT)$_n$, (dA)$_n$•2(dT)$_n$ → (dA)$_n$•(dT)$_n$ + (dT)$_n$) at lower salt concentrations. The close agreement we find between UV and DSC measurements at lower salt concentrations is similar to that reported for the (rA)$_n$,(rU)$_n$ system (Krakauer & Sturtevant, 1968).

Comparison of (dT)$_n$•2(dA)$_n$ with (rU)$_n$•2(rA)$_n$. Another triple-stranded helix containing two adenine residues, (rU)$_n$•2(rA)$_n$, was described by Broitman *et al.* (1987). (rU)$_n$•2(rA)$_n$ differs strikingly in its properties from (dT)$_n$•2(dA)$_n$. In contrast to (dT)$_n$•2(dA)$_n$, (rU)$_n$•2(rA)$_n$ is stable at low temperature and moderate ionic strength and upon heating is converted at moderate temperature to the double helix (rA)$_n$•(rU)$_n$ and (rA)$_n$. This behavior differs markedly from that of (dT)$_n$•2(dA)$_n$ which forms at high ionic strength from (dA)$_n$ and the double helix (dA)$_n$•(dT)$_n$ by an increase in temperature and, upon a further increase in temperature, is transformed to another triple helix, (dA)$_n$•2(dT)$_n$. The formation of (rU)$_n$•2(rA)$_n$ was reported by Broitman *et al.* (1987) to require a degree of polymerization of (rA)$_n$ of between 28 and 150. While not attempting to determine similar limits upon the formation of (dT)$_n$•2(dA)$_n$, we have failed to observe the formation of (dT)$_n$•2(dA)$_n$ with mixtures of oligomers at high ionic strength: with 20-mers of (dA)$_n$ and (dT)$_n$ tested with [NaCl] ranging to 4 M, with 16-mers to 5 M NaCl, and with dodecamers up to 3 M NaCl.

High-Temperature Melting of (dT)$_n$•2(dA)$_n$ Is Complex. Upon heating, 2 mol of the (dT)$_n$•2(dA)$_n$ triple helix transform to the familiar triple helix (dA)$_n$•2(dT)$_n$ and 3 mol of single-stranded (dA)$_n$ (eq 2). This reaction was identified from the mixing curves measured at 46 and 72 °C. The detailed mechanism by which (dT)$_n$•2(dA)$_n$ is converted to (dA)$_n$•2(dT)$_n$ and (dA)$_n$ is not known. It must necessarily involve, however, the dissociation of the third strand of (dA)$_n$:

$$[(dT)_n\cdot 2(dA)_n] \rightleftharpoons [(dA)_n\cdot(dT)_n] + (dA)_n \qquad (5)$$

Extrapolation of the ΔH_m of the formation reaction of eq 1 to 67 °C by use of the regression equation derived from the data of Table 1, and reversing the sign, leads to an estimate of $\Delta H_m = 1$ kcal mol^{-1} for eq 5. Tripling and adding this contribution to the observed value of $\Delta H_m = 4$ kcal mol^{-1} for the double disproportionation reaction (eq 3) give an estimate of $\Delta H_m = 7$ kcal mol^{-1} for the high temperature dissociation process, 2[(dT)$_n$•2(dA)$_n$] ⇌ (dA)$_n$•2(dT)$_n$ + 3(dA)$_n$, which is in agreement with the measured value of $\Delta H_m = 7.3$ kcal mol^{-1}. The thermodynamics of the high temperature dissociation of (dT)$_n$•2(dA)$_n$ (eq 2), therefore, can be accounted for in terms of the reactions of eqs 5 and 3. The bimodal appearance of the DSC traces and the slow kinetics implied by the scan rate dependence of the transition temperature of the high temperature triplex conversion reaction are wholly consistent with the representation of eq 2 as a complex process consisting of the constituent reactions expressed by eqs 5 and 3. These processes involve double helix dissociation and both third strand association and dissociation reactions, one or more of which might be responsible for the slow kinetic effects observed.

The double disproportionation reaction of (dA)$_n$•(dT)$_n$ to the two triple helices (eq 3) is also a complex reaction which formally involves dissociation of at least one A•T base pair and third strand addition reactions which may occur in a concerted manner through multistranded intermediates. The DSC trace for this process also appears bimodal, which reflects the complex nature of the process. Both high temperature transitions involving (dT)$_n$•2(dA)$_n$ as described by eqs 2 and 3 are complex processes in the sense that they are composed of more than one elementary reaction, that is, helix breaking and strand addition steps. The detailed mechanism of both of these multistep reactions is not understood.

Effect of Salt Concentration upon Thermal Stability of Complexes. At low to moderate salt concentrations (0.001−0.1 M NaCl), transition temperatures of polynucleotide helicies typically have a nearly linear dependence upon the logarithm of the electrolyte activity (Record *et al.*, 1978). The value of $dT_m/d \ln a_\pm$ is a characteristic property of a polynucleotide system and has been related to the amount of cation released or taken up during a transition through the equation:

$$\frac{dT_m}{d \ln a_\pm} = \frac{RT_m^2}{\Delta H}(\Delta i) \qquad (6)$$

where ΔH is the transition enthalpy, R is the gas constant, and Δi is the thermodynamic ion release (Krakauer & Sturtevant, 1968; Manning, 1972; Record *et al.*, 1978).

Formation of (dT)$_n$•2(dA)$_n$ from (dA)$_n$ and (dA)$_n$•(dT)$_n$ occurs only at high salt concentrations, however, over a range of 2.6−4.0 M NaCl. The transition temperature for formation has a strong inverse dependence upon ionic strength (T_m = 38.3 °C at 2.6 M NaCl, but only 13.9 °C at 4.0 M NaCl). A similar inverse dependence was observed for the melting

of DNA (Hamaguchi & Geiduschek, 1962). Robinson and Grant (1966) proposed that helix destabilization at high salt concentrations arises from the binding of anions to the exposed bases of the single strands, thus stabilizing the coiled forms relative to the helix. At high electrolyte concentrations the interpretation of Δi solely in terms of counterions is inadequate because anion and solvent interactions are neglected. A more complete description has been derived (Record *et al.*, 1978) for the helix to coil transition in a 1−1 electrolyte at high ionic strength:

$$\frac{dT_m}{d \ln a_\pm} = \frac{RT_m^2}{\Delta H}\left[\Delta n_M + \Delta n_X - \frac{2m}{55.6}(\Delta n_W) + \frac{d \ln(\gamma_D/\gamma_N)}{d \ln a_\pm}\right] \quad (7)$$

where Δn_W is the difference in moles of water bound per mole of nucleotide in the helix and coil forms and Δn_M and Δn_X are the corresponding quantities for cations and anions, m is the molality of simple salt, and γ_D and γ_N are activity coefficients of the denatured and native polynucleotide. For application to more complex reactions, for example, to eq 1, the quotient of activity coefficients in eq 7 must be appropriately modified. The parameter Z, defined as an experimental quantity in eq 4 above, is also identically the expression in brackets in eq 7, which contains the differential water, cation, and anion interaction terms.

For the formation of $(dT)_n{\cdot}2(dA)_n$ (eq 1) Z increases from −0.20 in 2.6−3.0 M NaCl to −0.09 in 3.8 M NaCl (Figure 11). This behavior can be qualitatively accounted for in terms of the parameters Δn_M, Δn_X, and Δn_W of eq 7. Formation of a triple helix with its high charge density results in a net uptake of cations. For the reaction $(dA)_n{\cdot}(dT)_n + (dT)_n \rightleftharpoons (dA)_n{\cdot}2(dT)_n$ in the vicinity of 0.1 M NaCl, for example, $\Delta i = -0.16$. By analogy, we suggest that the value $Z = -0.20$ for the formation of $(dT)_n{\cdot}2(dA)_n$ in 2.6−3.0 M NaCl also reflects, in part, the uptake of cations and implies that Δn_M is negative. Binding of Cl^- to $(dA)_n$ means that Δn_X is positive, and this effect tends to make Z more positive. Without this contribution, Z would be even more negative than −0.20. From the discussion of eq 7 by Record *et al.* (1978), we infer that, for the coil to helix transition of eq 1, Δn_W is positive, which also contributes (eq 7) to making Z negative.

With further increases in [NaCl], additional binding of Cl^- to $(dA)_n$ should lead to an increase in Δn_X, resulting in a more positive value of Z. Increased binding of Cl^- to $(dA)_n$, moreover, would also result in increased binding of Na^+ to $(dA)_n$ due to the increased negative charge (Record *et al.*, 1978), an effect that would also tend to make Z more positive. Increasingly higher salt concentrations may also reduce the amount of water bound to $(dA)_n$, so that when $(dA)_n$ reacts with $(dA)_n{\cdot}(dT)_n$, Δn_W is smaller than at lower salt concentrations, again making Z more positive (eq 7). We observe experimentally (Figure 11) that as [NaCl] increases to 3.8 M, Z increases to −0.09, in agreement with these predictions.

We suggest a similar interpretation applies to the conversion of $(dT)_n{\cdot}2(dT)_n$ to $(dA)_n{\cdot}2(dT)_n$ with release of single-stranded $(dA)_n$ (eq 2). At 2.6 M NaCl, $Z = 0.15$ (Figure 11); with increasing concentration of NaCl, enhanced binding of ions and water to $(dA)_n$ is expected to reduce Z; and indeed, we find that, at 4.0 M NaCl, $Z = -0.03$. In contrast, for the double disproportionation reaction in which the $(dA)_n{\cdot}(dT)_n$ double helix is converted to the two triple helices (eq 3) and in which single-stranded $(dA)_n$ is not involved, Z is independent of salt concentration. These results are consistent with and lend support to the proposal of Robinson and Grant (1966) regarding the binding of anions to the bases of single-stranded polynucleotides at high salt concentrations.

This discussion accounts qualitatively but not quantitatively for the observed behavior of Z.

Analysis of Effect of Salt Concentration of T_m and ΔH_m. A thermodynamic analysis of the experimental quantity $(dT_m/d \ln a_\pm)(\Delta H_m/RT_m^2) \equiv Z$ for the reaction processes of eqs 1−3 can be carried out in terms of the composite interaction parameter $\Delta\Gamma \equiv Z/2$. $\Delta\Gamma$ is the difference in Γ's between products and reactants, stoichiometrically weighted, where Γ is the Donnan membrane equilibrium parameter for each polynucleotide. The reactions of $(dT)_n{\cdot}2(dA)_n$, with the numerical subscripts of $\Delta\Gamma$ referring to eqs 1−3 and Γ expressed per mole of phosphorus, are:

$$\Delta\Gamma_1 = \Gamma_{AAT} - (2/3)\Gamma_{AT} - (1/3)\Gamma_A \quad (8a)$$

$$\Delta\Gamma_2 = (1/2)\Gamma_A + (1/2)\Gamma_{ATT} - \Gamma_{AAT} \quad (8b)$$

$$\Delta\Gamma_3 = (1/2)\Gamma_{AAT} + (1/2)\Gamma_{ATT} - \Gamma_{AT} \quad (8c)$$

The membrane equilibrium parameter Γ is defined as the difference in the normality of salt outside (C_s') and inside (C_s) a semipermeable membrane compartment containing polyelectrolyte divided by the monomer normality, n_p, at vanishing polymer concentration: $\Gamma \equiv \lim_{n_p \to 0} (C_s' - C_s)/n_p$. Experimentally, Γ is a positive quantity. Alternatively, Γ may be calculated from the Poisson−Boltzmann equation (PB) using a model requiring the input of the cylinder radius, the axial charge spacing, and the degree of ionization (Gross & Strauss, 1966; Bond *et al.*, 1994).

The dependence of Γ upon salt concentration has been accounted for by a model of the polyelectrolyte backbone and its surrounding ion atmosphere as a cylinder impenetrable to the added salt (Strauss & Ander, 1958). This model predicts that Γ will increase with C_s' as

$$\Gamma = (N_A \pi b C_s'/1000)(a + 1/\kappa)^2 \quad (9)$$

where N_A is Avogadro's number, b is the axial charge spacing, a is the cylinder radius, and the reciprocal Debye−Huckel length $\kappa = (8\pi e_0^2 C_s'/DkT)^{1/2}$, where e_0 is the electronic charge, D is the dielectric constant, and k is Boltzmann's constant.

Using eq 9 as a guide to extrapolate the membrane equilibrium data of NaDNA (Strauss *et al.*, 1967) to 3.4 M NaCl gives $\Gamma_{DNA} = 1.2$, and we estimate a closely similar value from the solution of the PB equation presented in Figure 2 of Bond *et al.* (1994). Therefore, the small $\Delta\Gamma$'s ($\leq |0.1|$) associated with our reactions in 2.6−4 M NaCl represent differences between typically large values of Γ. We assume that $(dA)_n{\cdot}(dT)_n$ has the same value of Γ as DNA (1.2) in 3.4 M NaCl, and we choose values for Γ of 1.3 and 1.1 for single- and triple-stranded polynucleotides, respectively, so that $\Delta\Gamma$ will be in approximate agreement with the analysis of DNA and $(rA)_n{\cdot}(rU)_n$ (Bond *et al.*, 1994). With

these values, the $\Delta\Gamma$'s calculated by eqs 8 are of the correct sign and similar to the values of $\Delta\Gamma$ that we have observed.

The variation of Γ with salt concentration, $d\Gamma/dC_s'$, and the rate of change of that variation, $d^2\Gamma/d^2C_s'$, according to eq 9, will depend upon the axial charge spacing, the cylinder radius, and the salt concentration. Thus, single-, double-, and triple-stranded polynucleotides will, in general, have different dependencies of Γ upon C_s'. As a consequence, $\Delta\Gamma$, formed by the addition of the Γ's of different polynucleotide species, may be ionic strength dependent. This reasoning would attribute the variation of Z ($2\Delta\Gamma$) with C_s' in Figure 11 to differences in the charge spacing and the cylindrical radii of the species involved.

This discussion indicates that the axial charge spacing and the space-filling effect of the hard cylinder can account for much of the behavior we have observed at high ionic strength. This treatment, however, does not explicitly include the anion binding suggested in the previous section.

Specific Anion Effects. The ability of anions to decrease helix stability follows the lyotropic series (von Hippel & Schleich, 1969), with highly polarizable anions such as ClO_4^- being more effective in lowering T_m than anions like Cl^- and Br^-. The enhanced binding the ClO_4^- to the exposed bases of (dA)$_n$ will shift the equilibrium of eq 1 farther to the left than will the less strongly interacting anions Cl^- and Br^-. We thus expect that (dT)$_n$•2(dA)$_n$ formation will be more adversely affected by ClO_4^- than by Cl^- or Br^-. The results shown in Figure 9 for the dependency of T_m upon salt concentration in NaCl, NaBr, and $NaClO_4$ solutions agree with this expectation. At low ($<\sim$0.2 M) salt concentration, the T_m's in NaCl, NaBr, and $NaClO_4$ are nearly the same; there are marked differences, however, at higher salt concentrations. Br^- is more polarizable than Cl^- and at higher anion concentration would be expected to interact more strongly with single-strand (dA)$_n$ than does Cl^-, so that Br^- disfavors formation of (dT)$_n$•2(dA)$_n$ more than does Cl^-. We find, in agreement with this expectation, that the temperature at which (dA)$_n$ reacts with (dA)$_n$•(dT)$_n$ to form (dT)$_n$•2(dA)$_n$ is about 12 °C higher when Br^- rather than Cl^- at the same anion concentration is present and that the temperature at which (dT)$_n$•2(dA)$_n$ melts is about 14 °C lower when Br^- rather then Cl^- is present. The still more polarizable ClO_4^- anion should have an even greater destablizing effect than Br^-. The results (Figure 9) indeed show that (dT)$_n$•2(dA)$_n$ is so disfavored that its formation does not occur in ClO_4^-.

This discussion and that of the two preceding sections indicate that single-stranded (dA)$_n$ and anions play an important role in determining the the behavior of the (dA)$_n$,(dT)$_n$ system at high salt.

It is of interest that Vorlickova *et al.* (1980) reported without comment a CD spectrum of a (dA)$_n$,(dT)$_n$ mixture at high concentrations of the weakly interacting F^- anion that resembles our spectrum of (dT)$_n$•2(dA)$_n$. We suggest that their spectrum indicates partial conversion to (dT)$_n$•2(dA)$_n$ in 6 M NaF.

Stability of (dT)$_n$•2(dA)$_n$. The (dT)$_n$•2(dA)$_n$ complex forms when mixtures of (dA)$_n$ and (dA)$_n$•(dT)$_n$ in NaCl at concentrations greater than 2.6 M are heated (Figures 5 and 7−10).

The DSC experiments provide quantitative thermodynamic information which accounts for many of the observed properties of (dT)$_n$•2(dA)$_n$. The favorable entropy change which drives the formation reaction is between 3.5 and 9 cal mol^{-1} K^{-1} and is offset by an unfavorable enthalpy change in the range of 1−2.5 kcal mol^{-1}. The formation of (dT)$_n$•2(dA)$_n$ is characterized by a negative heat capacity change, $\Delta C_p = -90$ cal mol^{-1} K^{-1}.

Formation of (dT)$_n$•2(dA)$_n$ is due to a favorable entropy change. Formation of a triple helix from a double helix and a random coil (eq 1) is not a process that would be entropically favorable from the point of view of change in mole number, reduction of chain conformational entropy, or the uptake of cations. The displacement of H_2O by the incoming third strand, the release of anions, preferentially interacting with single-stranded (dA)$_n$, and the release of previously electrostricted H_2O as a consequence of the uptake of cations by the new triple helix appear to be the most likely origins of the positive entropy change responsible for the formation of (dT)$_n$•2(dA)$_n$.

It is readily seen in the phase diagram of Figure 10 that (dT)$_n$•2(dA)$_n$ can only form and exist in a limited region of the temperature−NaCl plane: for example, the complex is stable in 3 M NaCl only in the temperature range between 25 and 60 °C. The stability of a biopolymer at a temperature, T, (assuming a temperature independent ΔC_p) is (Becktel & Schellman, 1987):

$$\Delta G^\circ(T) = \Delta H^\circ(\theta) - T\Delta S^\circ(\theta) + \Delta C_p[T - \theta - T\ln(T/\theta)] \quad (10)$$

where θ is an arbitrary reference temperature. The ΔC_p term introduces curvature into the free energy−temperature profile; and when the magnitude of this term is significant relative to that of $\Delta H^\circ(\theta)$, the dependence of the free energy function upon temperature has two roots where the biopolymer will have an upper and lower denaturation temperature in the observable temperature range, as does (dT)$_n$•2(dA)$_n$. Introducing the values of the thermodynamic parameters in Table 1 for the formation of this complex at low temperature into eq 10 leads to predicted values of the upper denaturation temperature to within 1 °C, on the average, for the data between 2.6 and 3.1 M NaCl. Equation 10, therefore, accounts semiquantitatively for the observed stability of this complex.

Simulation of the excess heat capacity curve using the values of the thermodynamic parameters obtained from fitting the low temperature transition in 2.6 M NaCl (Figure 7) accurately predicts the high temperature transition at 59.5 °C. The area under the high temperature peak is grossly underestimated in this simulation because the high temperature transition is not simply the reverse reaction of the low temperature transition but is complex and receives contributions to the enthalpy change from other reaction processes as discussed above. Thus, as a consequence of the small ΔH_m and large negative value of ΔC_p associated with its formation, (dT)$_n$•2(dA)$_n$ exhibits the phenomenon of "cold denaturation" as well as the more usual "melting" denaturation induced upon raising the temperature.

The principal thermodynamic result is that (dT)$_n$•2(dA)$_n$ is an extremely weak complex with a free energy of stabilization smaller than 100 cal mol^{-1}. The maximum stability of (dT)$_n$•2(dA)$_n$, according to eq 10, ranges from $\Delta G^\circ = -20$ cal mol^{-1} at 49 °C in 2.6 M NaCl to an estimate of $\Delta G^\circ = -100$ cal mol^{-1} at 41 °C in 3.4 M NaCl. As a consequence, the stability of (dT)$_n$•2(dA)$_n$ may be influenced by relatively subtle interactions. For example, anions can

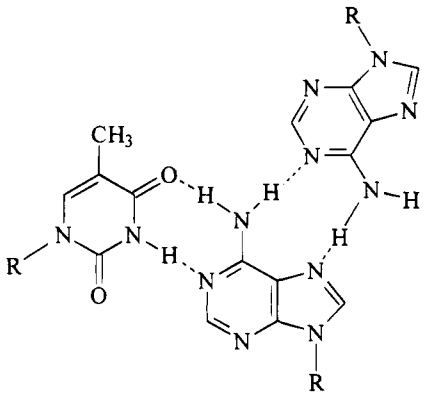

FIGURE 12: Proposed hydrogen-bonding scheme of $(dT)_n \cdot 2(dA)_n$.

play a decisive role in the formation of $(dT)_n \cdot 2(dA)_n$ as shown by the ability of the complex to form in NaCl and NaBr and by the complete inhibition of its formation in $NaClO_4$ (Figure 9). Anions, through their interaction with single-stranded $(dA)_n$, make an unfavorable contribution to the free energy of $(dT)_n \cdot 2(dA)_n$ formation, which in the case of ClO_4^- is sufficient to increase the intrinsically small free energy stabilizing $(dT)_n \cdot 2(dA)_n$ enough to make it positive and prevent its formation.

In a similar manner, a sufficiently long polynucleotide chain length may be required to overcome the intrinsically weak stability of $(dT)_n \cdot 2(dA)_n$, thus accounting for our failure to observe the formation of the $(dT)_n \cdot 2(dA)_n$ complex with oligomers.

Proposed Structure of $(dT)_n \cdot 2(dA)_n$. The hydrogen-bonding scheme we propose for the triple helix $(dT)_n \cdot 2(dA)_n$ is shown in Figure 12. The amino NH of the Watson–Crick (WC) adenine is bonded to N1 of the third strand adenine, and the 6NH of the latter is bonded to N7 of the WC A. The polarity of the two purine strands is antiparallel. An alternative scheme can be drawn in two dimensions with 6NH bonded to N7 of the third strand A and with the two purine strands parallel. Molecular modeling by V. Sasisekharan (personal communication), however, has shown that while a stereochemically satisfactory model can be constructed with antiparallel strands, parallel purine strands would require unacceptably short contacts.

While no direct experimental evidence exists for polarity of the third strand in the TAA case, there is evidence for analogous triple helices with mixed CT sequences paired (WC) to AG strands and a third strand of A and G paired (A to A; G to G) to the original WC purine strand. When the AG sequences in the third strand are chosen to be perfectly complementary if the purine strands are antiparallel, a stable triplex is formed. When the AG sequence is chosen to be complementary for parallel purine strands, no triple helix is formed (Pilch *et al.*, 1991; Rhadakrishnan *et al.*, 1991; Beal & Dervan, 1991; K. Liu and H. T. Miles, unpublished results). These experimental results are consistent with those of the model building by V. Sasisekharan in the TAA case.

The present report is relevant for Py•Pu•Pu triple helices in which the third strands contain A,G mixed sequences with A to A and G to G pairing. This study suggests that the stability of the mixed sequence triplexes, cited above, results largely from the GG interactions since, for the homopolymers reported here, the AA interaction is quite weak. For AG heteropolymers we suggest that the AA pairing is similarly weak, although it may make an important contribution to the stability by diluting the runs of G and preventing G-tetramer formation at the expense of triple helix formation.

REFERENCES

Archer, D. G. (1992) *J. Phys. Chem. Ref. Data 21*, 793–821.

Arnott, S., & Selsing, E. (1974) *J. Mol. Biol. 88*, 509–521.

Beal, P. A., & Dervan, P. B. (1991) *Science 251*, 1360–1363.

Becktel, W. J., & Schellman, J. A. (1987) *Biopolymers 26*, 1859–1877.

Bond, J. P., Anderson, C. F., & Record, M. T., Jr. (1994) *Biophys. J. 67*, 825–836.

Broitman, S. L., Im, D. D. & Fresco, J. R. (1987) *Proc. Natl. Acad. Sci. U.S.A. 84*, 5120–5124.

Felsenfeld, G., Davies, D. R., & Rich, A. (1957) *J. Am. Chem. Soc. 79*, 2023–2024.

Gross, L. M., & Strauss, U. P. (1966) in *Chemical Physics of Ionic Solutions* (Conway, B. E., & Barradas, R. G., Eds.) pp 361–384, John Wiley & Sons, New York.

Hamaguchi, K., & Geiduschek, E. P. (1962) *J. Am. Chem. Soc. 84*, 1329–1338.

Howard, F. B., & Miles, H. T. (1984) *Biochemistry 23*, 6723–6732.

Howard, F. B., Frazier, J., & Miles, H. T. (1976) *Biochemistry 15*, 3783–3795.

Howard, F. B., Miles, H. T., Liu, K., Frazier, J., Raghunathan, G., & Sasisekharan, V. (1992) *Biochemistry 31*, 10671–10677.

Job, P. (1928) *Ann. Chim. (Paris) 9*, 113–134.

Kirchoff, W. H. (1993) *EXAM: A Two-State Thermodynamic Analysis Program*, NIST Technical Note 1401, U.S. Department of Commerce, Gaithersburg, MD.

Krakauer, H., & Sturtevant, J. M. (1968) *Biopolymers 6*, 491–512.

Manning, G. S. (1972) *Biopolymers 11*, 937–959.

Muraoka, M., Miles, H. T., & Howard, F. B. (1980) *Biochemistry 19*, 2429–2439.

Pilch, D. S., Lenenson, C. & Shafer, R. H. (1991) *Biochemistry 30*, 6081–6087.

Powell, J. I., Fico, R., Jennings, W. H., O'Bryan, E. R., & Schultz, A. R. (1980) Proceedings of the IEEE Computer Society, 21st International Conference, pp 185–190, IEEE Computer Society, Los Angeles, CA.

Radhakrishnan, I., de los Santos, C., & Patel, D. J. (1991) *J. Mol. Biol. 221*, 1403–1418.

Record, M. T., Jr., Anderson, C. F., & Lohman, T. M. (1978) *Q. Rev. Biophys. 11*, 103–178.

Riley, M., Maling, B., & Chamberlin, M. J. (1966) *J. Mol. Biol. 20*, 359–389.

Robinson, D. R., & Grant, M. E. (1966) *J. Biol. Chem. 241*, 4030–4042.

Strauss, U. P., & Ander, P. (1958) *J. Am. Chem. Soc. 80*, 6494–6498.

Strauss, U. P., Helfgott, C., & Pink, H. (1967) *J. Phys. Chem. 71*, 2550–2556.

von Hippel, P. H., & Schleich, T. (1969) in *Biological Macromolecules, Vol. 2, Structure and Stability of Biological Macromolecules* (Timasheff, S. N., & Fasman, G., Eds.) pp 417–574, Marcel Dekker, New York.

Vorlickova, M., Kypr, J., Kleinwachter, V., & Palecek, E. (1980) *Nucleic Acids Res. 8*, 3965–3973.

BI950055R